Nonlinear Thermal Radiation and Chemical Reaction Effects on a (Cu?CuO)/NaAlg Hybrid Nanofluid Flow Past a Stretching Curved Surface

Authors:

Naveed Ahmed, Fitnat Saba, Umar Khan, Syed Tauseef Mohyud-Din, El-Sayed M. Sherif, Ilyas Khan

Abstract:

The boundary layer flow of sodium alginate (NaAlg) based (Cu ? CuO) hybrid nanofluid, over a curved expanding surface, has been investigated. Heat and mass transport phenomena have also been analyzed. Moreover, the impacts of chemical reaction, magnetic field and nonlinear thermal radiation are also a part of this study. This arrangement has great practical relevance, especially in the polymer and chemical industries. We have extended the Bruggeman model to make it capable of capturing the thermal conductivity of (Cu ? CuO) / NaAlg hybrid nanofluid. We have employed some suitable transformations to obtain the governing system of nonlinear ODEs. Runge ? Kutta ? Fehlberg algorithm, accompanied by a shooting technique, has been employed to solve the governing system numerically. The changes in the flow and heat transfer distribution, due to various parameters, have been captured and portrayed in the form of graphs. It has been found that the addition of the nanometer-sized materials, significantly boosts the thermal and heat transport properties of the host fluid, and these phenomena seem to be more prominent, in the case of (Cu ? CuO) / NaAlg hybrid nanofluid.

Record Type: Published Article

Nonlinear Thermal Radiation and Chemical Reaction Effects on a (Cu−CuO)/NaAlg Hybrid Nanofluid Flow Past a Stretching Curved Surface

Naveed Ahmed [1] , **Fitnat Saba** [1], **Umar Khan** [2] , **Syed Tauseef Mohyud-Din** [1],
El-Sayed M. Sherif [3,4] **and Ilyas Khan** [5,*]

[1] Department of Mathematics, Faculty of Sciences, HITEC University, Taxila Cantt, Rawalpindi 47080, Pakistan; nidojan@gmail.com (N.A.); fitnat_saba89@gmail.com (F.S.); syedtauseefs@hotmail.com (S.T.M.-D.)

[2] Department of Mathematics and Statistics, Hazara University, Mansehra 21120, Pakistan; umar_jadoon4@yahoo.com

[3] Center of Excellence for Research in Engineering Materials (CEREM), King Saud University, P.O. Box 800, Al-Riyadh 11421, Saudi Arabia; esherif@ksu.edu.sa

[4] Electrochemistry and Corrosion Laboratory, Department of Physical Chemistry, National Research Centre, El-Behoth St. 33, Dokki, Cairo 12622, Egypt

[5] Faculty of Mathematics and Statistics, Ton Duc Thang University, Ho Chi Minh City 72915, Vietnam

* Correspondence: ilyaskhan@tdtu.edu.vn

Abstract: The boundary layer flow of sodium alginate (NaAlg) based (Cu − CuO) hybrid nanofluid, over a curved expanding surface, has been investigated. Heat and mass transport phenomena have also been analyzed. Moreover, the impacts of chemical reaction, magnetic field and nonlinear thermal radiation are also a part of this study. This arrangement has great practical relevance, especially in the polymer and chemical industries. We have extended the Bruggeman model to make it capable of capturing the thermal conductivity of (Cu − CuO)/NaAlg hybrid nanofluid. We have employed some suitable transformations to obtain the governing system of nonlinear ODEs. Runge−Kutta−Fehlberg algorithm, accompanied by a shooting technique, has been employed to solve the governing system numerically. The changes in the flow and heat transfer distribution, due to various parameters, have been captured and portrayed in the form of graphs. It has been found that the addition of the nanometer-sized materials, significantly boosts the thermal and heat transport properties of the host fluid, and these phenomena seem to be more prominent, in the case of (Cu − CuO)/NaAlg hybrid nanofluid.

Keywords: (Cu−CuO)/NaAlg hybrid nanofluid; curved stretching surface; boundary layer; nonlinear thermal radiation; heat and mass transfer; chemical reaction; numerical results

---

1. Introduction

It has been more than twenty years since a new generation of functional operating fluids, named as 'Nanofluids' have been discovered. The colloids have been accomplished by adding nanometer-sized structures (size less than 100 nm), within the conventional single-phase fluids. The single-phase heat transfer liquids like water, sodium alginate, lubricants, engine oil, organic liquids (e.g., propylene and ethylene glycols, etc.) and polymeric solutions, seems deficient to intensify the heat transmission rate, in various engineering and industrial processes. The leading cause behind is the least effective thermal properties of the working fluids. Nano additives significantly boost the thermal properties of the single-phase fluids [1]. In this regard, the pioneering

work has been delivered by Choi [2,3], which significantly highlights the existence and effectiveness of tiny sized particles on the thermal efficiency of the single-phase heat transfer fluids. Later on, numerous research activities have been carried out by a number of scientists. Subsequently, a variety of models, related to the thermo-mechanical properties of nanofluids, have been introduced, for numerous industrial and practical situations. In this context, Maxwell [4] announced a model that is based on the thermal conductivities of single-phase fluids along with the solid nanocomposites. Besides, this method deals explicitly with the spherical shaped tiny composites, whose volume concentration is assumed to be very small. Afterwards, a theoretical model has been developed by Bruggeman [5], which usually encounters the relationships between the spheres shaped solid nanocomposites. In 1962, Hamilton and Crosser [6] reformulated Maxwell's model by introducing the shape factor. Further studies, in this field, reveal several mechanisms [7–11] that can be helpful in improving the thermal efficiency of nanofluids.

Nanofluids have replaced the conventional single-phase heat transfer fluids in numerous applications including car radiators, oil recovery, aerospace engineering, lubrication, the system of photovoltaic and solar collectors, drug delivery, medicine, cooling of electronic systems, etc. During the last two decades, a number of research activities related to the preparation, classification, dispersion, modelling and rate of heat transfer due to convection, in the case of mono nanofluids, have been conducted, which makes a significant contribution in the existing literature [1]. Recently, a novel subject of hybrid nanofluid, successfully caught the sights of worldwide researchers, due to their superior thermo-mechanical properties, when compared to monotype nanofluids. The hybrid composition has been accomplished by dispersing (i) a variety (two or more) of nanometer-sized particles in the single-phase liquids, and (ii) composite nanostructures in the single-phase heat transfer fluids. Thus, the process of hybridization successfully leads to the homogenous phase, which provides the physical and chemical bonding of several materials at one place. The purpose of hybridity is to boost the characteristic features, like thermomechanical, hydrodynamic and heat transport properties of traditionally used fluids [12,13].

The innovative concept of hybrid nanofluid has a profound impact on the global research community and consequently, the research activities, in this area, have shown immense progress, during the last few years [13]. By opting the novel idea of material design, Niihara [14] incorporated the nanometer-sized particles within the host fluid and hence, gave a detailed description related to the improvement in the physical and chemical characteristics of the host fluid. Jana et al. [15] introduced the mono and hybrid type nanofluids to inspect the thermal efficiency of the common fluid. By considering the two-step procedure, Suresh et al. [16] critically scrutinized the behavior of $(AI_2O_3 - Cu)$/water hybrid nanofluid. They have provided an experimental result, which exhibits an increment in the viscosity along with the thermal conductivity of the host fluid. In another study [17], they have presented a brief explanation regarding the heat transport properties of $(AI_2O_3 - Cu)$/water hybrid nanofluid. By making use of a numerical scheme, Balla et al. [18] investigated the augmentation in the heat transport mechanism, for hybrid $(CuO - Cu)$ nanofluid. By taking the different shapes of nanocomposites into consideration, Saba et al. [19] explored the thermophysical properties of H_2O based hybrid $(Cu - AI_2O_3)$ nanofluid in an asymmetric channel. Recently, Ahmed et al. [20] presents a study, comprising the combined effects of nonlinear thermal radiation and chemical reaction, on the squeezing flow of H_2O based hybrid $(Ag - Fe_3O_4)$ nanofluid between two Riga plates.

In recent past years, the worldwide-renowned scientists have paid immense attention to the study of the flows over flat expanding surfaces. These kinds of flows have paved a way in many industrial and engineering processes such as paper manufacturing, polymer sheets, production of plastic and rubber sheets, wire coating, glass fibers, food manufacturing processes, etc. In this context, Sakiadis [21] was a pioneer, who firstly introduced the concept of flows of boundary layer nature, over a flat expanding surface. Then, his concept has been utilized by Crane [22], who considered the flow due to the linear stretching of the flat surface. These pioneering works then paved the way for the worldwide scientists, to discover the new ideas related to this interesting subject. Later, Gupta and

Gupta [23] presented a remarkable work by considering the flow behavior over a spongy surface. After the pioneering work, to date, many scientists have encountered a variety of flow situations related to the study of the flat stretching surface [24–26] and the references therein.

In modern adhesive cutting-edge technology, the stretching of curved surfaces has found a way in many practical applications, for example, in electronics, transportation, etc. However, the subject related to the flow caused by the stretching of the curved surface has been hardly attended. In 2010, Sajid et al. [27], for the very first time, scrutinized the viscid flow over a curved expanding surface, which can be stretched with the linear velocity. They have also revealed through their study that the thickness of the boundary layer boosts in the case of a curved stretching surface when compared with the flat stretching surface. By taking the magnetohydrodynamic effects into account, Hayat et al. [28] examined the nonlinear thermal radiative effects, on the flow of nanofluid, with copper and silver are taken as nano additives, over the curved stretching surface. They have also analyzed the heat transport mechanism due to the convective process. By employing carbon nanotubes in the host fluid, Saba and her fellows [29] briefly analyzed the flow behavior over a curved surface. They have also examined the system of heat transport under the action of radiative effects together with the internal generation of heat. Lu et al. [30] investigated the hybrid nano liquid flow under the influence of various embedded factors like a magnetic field, nonlinear thermal radiation and heat absorption/generation. They have also inspected the mass and heat transport phenomena during their study.

Heat radiation is a procedure of transferring internal energy via electromagnetic waves. The infrared region comprises all those objects, from the earth's surface, that emits the radiative energy. The thermal radiation has a wide range of applications such as glass manufacturing, polymer processing, solar power plant, thermal storage compounds, electrical power production, nuclear power technology and numerous industrial areas. Magnetohydrodynamics characterizes the flow behavior of fluids, possessing the electrical conducting properties, under the action of an externally applied magnetic field. Numerous engineering and industrial applications including power generators, pumps, heat exchangers, accelerators and the cooling reactors involve the magnetohydrodynamics systems. Reddy [31] employed the magnetohydrodynamics along with thermal radiative effects, to briefly discussed the behavior of a nanofluid flow, over a linearly stretching surface. The impact of radiation and externally applied magnetic field on the nanofluids over a nonlinear stretching surface has been analyzed by Poornima and Reddy [32]. Some other studies comprising the magnetohydrodynamics along with thermal radiative effects can be found in [33,34] and the references therein.

On reviewing the existing literature, copious research activities have been found on the subject of nanofluids, over a flat stretchable surface; however, the articles related to the curved expanding surfaces are limited in number. This number gets even narrower, when the topic of a hybrid nanofluid, over a curved stretching surface, came under discussion. Therefore, the main concern of this article is to discuss the sodium alginate (NaAlg) based (Cu − CuO) hybrid nanofluid, over a stretchable curved surface. The whole analysis has been carried out with additional factors such as nonlinear thermal radiation, magnetohydrodynamics and chemical reaction effects. Heat and mass transport mechanisms have also been analyzed in details. Numerical results for the envisioned model have been developed by implementing a numerical recipe, so-called Runge−Kutta−Fehlberg algorithm accompanied by the shooting technique. The graphical simulation along with a detail physical description has also been provided, that significantly highlights the traits of various meaningful emerging entities on the involved distributions.

2. Thermophysical Traits of Hybrid Nanofluid

In this analysis, at an initial stage, the nanometer-sized particles of CuO have been added into the sodium alginate (NaAlg), to form the regular CuO/NaAlg nanofluid. Then copper (Cu) nanocomposites have been employed, with varying volumetric fractions, to achieve the configuration

of sodium alginate (NaAlg) based (Cu − CuO) hybrid nanofluid. In the case of hybrid nanofluid, the volumetric fraction of nanometer-sized small particles can be defined by the following expression [18]:

$$\Phi_{hnf} = \frac{Vol_{Cu} + Vol_{CuO}}{Vol_{total}} = \Phi_1 + \Phi_2. \tag{1}$$

To estimate the thermophysical properties, corresponding to the mono and hybrid nanofluids, the nano additives were supposed to be uniformly distributed in the host fluid. A number of correlations, defining the thermophysical traits of mono nanofluid, have been proposed by many scientists, whose results were well matched with the experimental outcomes. In comparison to this, the empirical correlations, relative to the thermophysical traits of hybrid nanofluid, are limited in number. Therefore, this segment has been designed for the correlations, which can be used for estimating the viscosity, density, specific heat, electrical and thermal conductivity of the hybrid nanofluid [13].

2.1. Viscosity

In real-life situations, the credibility of the nanofluid is greatly challenged by copious factors, including friction forces, pressure variations, and consequently pumping powers. Therefore, the importance of the viscosity of a mono nanofluid cannot be neglected. Brinkman [11], in 1952, suggested a correlation for the estimation of dynamic viscosity of regular nanofluid $\left(\hat{\mu}_{nf}\right)$, which is defined as:

$$\hat{\mu}_{nf} = \hat{\mu}_f \left(1 - \Phi_1\right)^{-25/10}, \tag{2}$$

where, $\hat{\mu}_f$ symbolizes the dynamic viscosity of the host fluid. On the basis of mixture formula, the dynamic viscosity for hybrid nanofluid $\left(\hat{\mu}_{hnf}\right)$ is defined as [12,19]:

$$\hat{\mu}_{hnf} = \hat{\mu}_{nf} \left(1 - \Phi_2\right)^{-25/10}. \tag{3}$$

2.2. Density

Pak with his fellow workers [7] derived a model for calculating the density of regular nanofluid, denoted by $\hat{\rho}_{nf}$, which is given as:

$$\hat{\rho}_{nf} = \left\{ \hat{\rho}_f - \Phi_1 \left(\hat{\rho}_f - \hat{\rho}_{s1} \right) \right\}, \tag{4}$$

where, $\hat{\rho}_f$ represents the density of a host fluid. By employing the same mixture formula, the density $\left(\hat{\rho}_{hnf}\right)$, in the case of hybrid nanofluid, is given by the following expression [12,19]:

$$\hat{\rho}_{hnf} = \hat{\rho}_{s2}\Phi_2 + \left(1 - \Phi_2\right)\left\{ \hat{\rho}_f - \Phi_1 \left(\hat{\rho}_f - \hat{\rho}_{s1} \right) \right\}. \tag{5}$$

2.3. Heat Capacity

In the case of regular nanofluids, the correlation for heat capacity $\left(\hat{\rho}\hat{C}_p\right)_{nf}$ was offered by Pak et al. [7], which can be mathematically expressed as [12,19]:

$$\left(\hat{\rho}\hat{C}_p\right)_{nf} = \left\{ \left(\hat{\rho}\hat{C}_p\right)_f - \Phi_1\left(\left(\hat{\rho}\hat{C}_p\right)_f - \left(\hat{\rho}\hat{C}_p\right)_{s1}\right) \right\}, \tag{6}$$

where, $\left(\hat{\rho}\hat{C}_p\right)_f$ illustrates the heat capacity of a host fluid. By the same mixture principal, the heat capacity for hybrid nanofluid $\left(\hat{\rho}\hat{C}_p\right)_{hnf}$ can be computed through the following correlation:

$$\left(\hat{\rho}\hat{C}_p\right)_{hnf} = \left(\hat{\rho}\hat{C}_p\right)_{s2}\Phi_2 + \left(1 - \Phi_2\right)\left\{ \left(\hat{\rho}\hat{C}_p\right)_f - \Phi_1\left(\left(\hat{\rho}\hat{C}_p\right)_f - \left(\hat{\rho}\hat{C}_p\right)_{s1}\right) \right\}. \tag{7}$$

2.4. Electrical Conductivity

The following correlations can be utilized for the estimation of electrical conductivity, for both mono and hybrid nanofluids, which can be given by [12]:

$$\hat{\sigma}_{nf} = \hat{\sigma}_f \frac{\hat{\sigma}_{s1}(2\Phi_1 + 1) - 2\hat{\sigma}_f(\Phi_1 - 1)}{\hat{\sigma}_f(\Phi_1 + 2) - \hat{\sigma}_{s1}(\Phi_1 - 1)}, \tag{8}$$

$$\hat{\sigma}_{hnf} = \hat{\sigma}_f \frac{\hat{\sigma}_{s1}(2\Phi_1 + 1) - 2\hat{\sigma}_f(\Phi_1 - 1)/\hat{\sigma}_{nf}(\Phi_2 + 2) - \hat{\sigma}_{s2}(\Phi_2 - 1)}{\hat{\sigma}_f(\Phi_1 + 2) - \hat{\sigma}_{s1}(\Phi_1 - 1)/\hat{\sigma}_{s2}(2\Phi_2 + 1) - 2\hat{\sigma}_{nf}(\Phi_2 - 1)}. \tag{9}$$

2.5. Thermal Conductivity

It is one of the prime thermophysical traits, which plays a counterpart in improving the heat transport mechanism, in the case of a regular nanofluid. The suspension of nano additives, bearing highly thermal conductive properties, can significantly enhance the thermal efficiency of regular nanofluid, which is mainly due to the convective transport of current between the host fluid and solid nanomaterials. The same reason goes for hybrid nanofluids as well. Existing literature provides a number of theoretical models that can effectively predict the thermal conductivity of nanofluids. In this context, the coined work of Maxwell [4] offered a theoretical model, which is effectively valid for the low concentration of nanomaterials. Mathematically:

$$\hat{K}_{nf} = \hat{K}_f \frac{\hat{K}_{s1}(2\Phi_1 + 1) - 2\hat{K}_f(\Phi_1 - 1)}{\hat{K}_f(\Phi_1 + 2) - \hat{K}_{s1}(\Phi_1 - 1)}. \tag{10}$$

In the case of hybrid nanofluid, it can be adapted as [12,13,19,20]:

$$\hat{K}_{hnf} = \hat{K}_{nf} \frac{\hat{K}_{s2}(2\Phi_2 + 1) - 2\hat{K}_{nf}(\Phi_2 - 1)}{\hat{K}_{nf}(\Phi_2 + 2) - \hat{K}_{s2}(\Phi_2 - 1)}. \tag{11}$$

In 1935, Bruggeman [5] developed a correlation, which is valid for the spherical shaped nanometers sized structures and, can be employed for any %V/V. For regular nanofluid, it can be defined as:

$$\hat{K}_{nf} = \frac{\hat{K}_f}{4}\left[(3\Phi_1 - 1)\left(\frac{\hat{K}_{s1}}{\hat{K}_f}\right) - (3\Phi_1 - 2) + (\Delta_1)^{0.5}\right], \tag{12}$$

where,

$$\Delta_1 = \left[(3\Phi_1 - 1)^2\left(\frac{\hat{K}_{s1}}{\hat{K}_f}\right)^2 + (2 - 3\Phi_1)^2 + 2(2 + 9\Phi_1 - 9\Phi_1^2)\left(\frac{\hat{K}_{s1}}{\hat{K}_f}\right)\right], \tag{13}$$

where, $\hat{K}_f$ denotes the thermal conductivity of a host fluid. Furthermore, by following the mixture formula, the Bruggeman model can be upgraded for the hybrid nanofluid, which can be written as [13,20,35]:

$$\hat{K}_{hnf} = \frac{\hat{K}_{nf}}{4}\left[(3\Phi_2 - 1)\left(\frac{\hat{K}_{s2}}{\hat{K}_{nf}}\right) - (3\Phi_2 - 2) + (\Delta_2)^{0.5}\right], \tag{14}$$

where,

$$\Delta_2 = \left[(3\Phi_2 - 1)^2\left(\frac{\hat{K}_{s2}}{\hat{K}_{nf}}\right)^2 + (2 - 3\Phi_2)^2 + 2(2 + 9\Phi_2 - 9\Phi_2^2)\left(\frac{\hat{K}_{s2}}{\hat{K}_{nf}}\right)\right]. \tag{15}$$

2.6. Mass Diffusivity

By making use of the mixture formula, the correlation expressions for the mass diffusivity, for both mono and hybrid nanofluids, are simultaneously defined as [8,20,36]:

$$\hat{\mathbb{D}}_{nf} = \left(1 - \Phi_1\right)\hat{\mathbb{D}}_f, \tag{16}$$

$$\hat{\mathbb{D}}_{hnf} = \left(1 - \Phi_2\right)\hat{\mathbb{D}}_{nf}. \tag{17}$$

In the equations mentioned above ((1)–(17)), Φ_1 and Φ_2 simultaneously show the volumetric fractions of CuO and Cu nanoadditives. The subscript $s1$ and $s2$ stands for CuO and Cu nanocomposites. The thermophysical traits associated with the host fluid (sodium alginate) and the nano additives (CuO and Cu) are appended in Table 1.

Table 1. Thermo-physical properties (electrical conductivity, thermal conductivity, heat capacity and density) of the base fluid (Sodium alginate) and nano additives (CuO and Cu) [9,10].

Physical Properties	Base Fluid	Nanoadditives	
	NaAlg (f)	CuO	Cu
$\hat{\sigma}\left(\Omega^{-1}\mathrm{m}^{-1}\right)$	2.6×10^{-4}	2.7×10^{-8}	5.96×10^{7}
$\hat{K}\left(\mathrm{WK}^{-1}\mathrm{m}^{-1}\right)$	0.6376	76.5	401
$\hat{C}_p\left(\mathrm{J\,K}^{-1}\mathrm{kg}^{-1}\right)$	4175	531.8	385
$\hat{\rho}\left(\mathrm{kg\,m}^{-3}\right)$	989	6320	8933

3. Problem Formulation in Curvilinear Coordinates

A time-independent, incompressible, laminar flow of sodium alginate $\left(\mathrm{NaAlg}\right)$ based $\left(\mathrm{Cu} - \mathrm{CuO}\right)$ hybrid nanofluid, moving over a curved surface, at $\hat{\mathbb{r}} = \hat{\mathbb{R}}$, has been under consideration (see Figure 1). The curved surface endures a linear stretchable velocity $\left(\hat{\mathbb{U}} = \hat{a}_1\hat{\mathbb{s}} \text{ with } \hat{a}_1 > 0\right)$ in the horizontal $\left(\hat{\mathbb{s}}\right)$ direction, while, a boundary layer has been established by the fluid, in the radial ($\hat{\mathbb{r}}$) direction. The curvy shape of the surface can be determined via $\hat{\mathbb{R}}$, the distance between the surface to the origin, and the curved surface become flat, for an infinitely large radius of curvature $\left(\hat{\mathbb{R}}\right)$. The constant magnetic field, with strength $\hat{B}_0$, is also employed, which acts normal to the fluid flow, i.e., in the radial $\left(\hat{\mathbb{r}}\right)$ direction. By owing the assumption of small Reynolds number, all the impacts due to electric and induced magnetic fields are neglected. Furthermore, heat and mass transport mechanisms are examined through nonlinear thermal radiation and chemical reaction. It is further pertinent to mention that the temperature along with concentration are simultaneously represented by $\hat{\mathcal{T}}_w$ and $\hat{\mathbb{C}}_w$, while, $\hat{\mathcal{T}}_\infty$ and $\hat{\mathbb{C}}_\infty$ corresponds to the temperature and concentration of free streamlines with the assumptions $\hat{\mathcal{T}}_\infty < \hat{\mathcal{T}}_w$ and $\hat{\mathbb{C}}_\infty < \hat{\mathbb{C}}_w$.
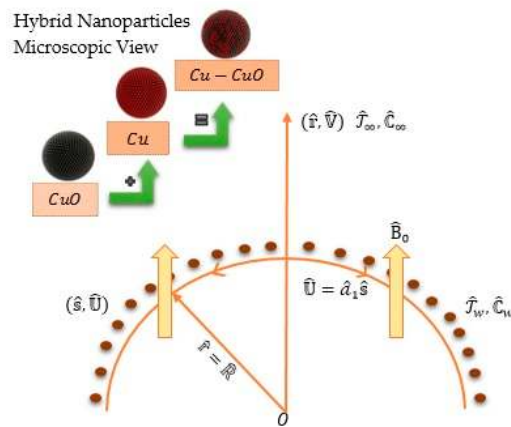
Figure 1. Geometrical illustration of the boundary layer flow problem.

Under the assumptions as mentioned above, the governing equations, including the continuity, momentum, temperature and concentration profiles, relevant to the current boundary layer flow situation, can be mathematically expressed as follows [28,30]:

$$\frac{1}{\hat{\mathbb{R}}}\frac{\partial}{\partial\hat{\mathbb{r}}}\left(\Lambda\hat{\mathbb{V}}\right)+\frac{\partial\hat{\mathbb{U}}}{\partial\hat{\mathbb{s}}}=0, \tag{18}$$

$$\frac{1}{\hat{\rho}_{hnf}}\frac{\partial\hat{\mathbb{P}}}{\partial\hat{\mathbb{r}}}-\frac{\hat{\mathbb{U}}^2}{\Lambda}=0, \tag{19}$$

$$\frac{1}{\hat{\rho}_{hnf}}\frac{\hat{\mathbb{R}}}{\Lambda}\frac{\partial\hat{\mathbb{P}}}{\partial\hat{\mathbb{s}}}+\left(\frac{\partial\hat{\mathbb{U}}}{\partial\hat{\mathbb{r}}}\hat{\mathbb{V}}+\frac{\hat{\mathbb{R}}}{\Lambda}\frac{\partial\hat{\mathbb{U}}}{\partial\hat{\mathbb{s}}}\hat{\mathbb{U}}+\frac{1}{\Lambda}\hat{\mathbb{V}}\hat{\mathbb{U}}\right)=\hat{v}_{hnf}\left\{\frac{\partial^2\hat{\mathbb{U}}}{\partial\hat{\mathbb{r}}^2}+\frac{1}{\Lambda}\frac{\partial\hat{\mathbb{U}}}{\partial\hat{\mathbb{r}}}-\frac{\hat{\mathbb{U}}}{\Lambda^2}\right\}-\frac{\hat{\sigma}_{hnf}}{\hat{\rho}_{hnf}}\hat{B}_0^2\hat{\mathbb{U}}, \tag{20}$$

$$\left(\hat{\rho}\hat{C}_p\right)_{hnf}\left(\frac{\partial\hat{\mathscr{T}}}{\partial\hat{\mathbb{r}}}\hat{\mathbb{V}}+\frac{\hat{\mathbb{R}}}{\Lambda}\frac{\partial\hat{\mathscr{T}}}{\partial\hat{\mathbb{s}}}\hat{\mathbb{U}}\right)+\frac{1}{\Lambda}\frac{\partial}{\partial\hat{\mathbb{r}}}\left(\Lambda\hat{\mathbb{q}}_{\hat{\mathbb{r}}}\right)=\frac{\hat{K}_{hnf}}{\Lambda}\left[\left(\frac{\partial\hat{\mathscr{T}}}{\partial\hat{\mathbb{r}}}+\Lambda\frac{\partial^2\hat{\mathscr{T}}}{\partial\hat{\mathbb{r}}^2}\right)\right], \tag{21}$$

$$\left(\frac{\partial\hat{\mathbb{C}}}{\partial\hat{\mathbb{r}}}\hat{\mathbb{V}}+\frac{\hat{\mathbb{R}}}{\Lambda}\frac{\partial\hat{\mathbb{C}}}{\partial\hat{\mathbb{s}}}\hat{\mathbb{U}}\right)=\frac{\hat{\mathbb{D}}_{hnf}}{\Lambda}\left[\left(\frac{\partial\hat{\mathbb{C}}}{\partial\hat{\mathbb{r}}}+\Lambda\frac{\partial^2\hat{\mathbb{C}}}{\partial\hat{\mathbb{r}}^2}\right)\right]-\hat{c}_0\left(\hat{\mathbb{C}}-\hat{\mathbb{C}}_\infty\right), \tag{22}$$

where $\Lambda=\hat{\mathbb{r}}+\hat{\mathbb{R}}$. $\hat{\mathbb{U}}$ and $\hat{\mathbb{V}}$ simultaneously depict the horizontal $\left(\hat{\mathbb{s}}\right)$ and radial $\left(\hat{\mathbb{r}}\right)$ velocity components. $\hat{\rho}_{hnf}$, $\hat{\sigma}_{hnf}$ and $\hat{v}_{hnf}$ symbolizes the density, electrical conductivity and kinematic viscosity for the hybrid nanofluid, respectively. The heat capacity, thermal conductivity and thermal diffusivity, in the case of hybrid nanofluid, are respectively denoted by $\left(\hat{\rho}\hat{C}_p\right)_{hnf}$, $\hat{K}_{hnf}$ and $\hat{\mathbb{D}}_{hnf}$. Moreover, $\hat{\mathbb{P}}$ stands for the pressure term, while, the temperature and concentration are simultaneously represented by $\hat{\mathscr{T}}$ and $\hat{\mathbb{C}}$. The radiative term is indicated by $\hat{\mathbb{q}}_{\hat{\mathbb{r}}}$, while $\hat{c}_0$ illustrates the chemical reaction.

The relevant boundary conditions are defined as [28,30]:

$$\hat{\mathbb{U}}\bigg|_{\hat{\mathbb{r}}=0}=\hat{\mathbb{U}}_w\left(\hat{\mathbb{s}}\right)=\hat{a}_1\hat{\mathbb{s}},\ \hat{\mathbb{V}}\bigg|_{\hat{\mathbb{r}}=0}=0,\ \hat{\mathscr{T}}\big|_{\hat{\mathbb{r}}=0}=\hat{\mathscr{T}}_w,\ \hat{\mathbb{C}}\bigg|_{\hat{\mathbb{r}}=0}=\hat{\mathbb{C}}_w,$$

$$\hat{\mathbb{U}}\Big|_{\hat{\mathbb{r}}\to\infty}\to 0,\ \ \frac{\partial\hat{\mathbb{U}}}{\partial\hat{\mathbb{r}}}\Bigg|_{\hat{\mathbb{r}}\to\infty}\to 0,\ \ \hat{\mathscr{T}}\Big|_{\hat{\mathbb{r}}\to\infty}\to\hat{\mathscr{T}}_{\infty},\ \ \hat{\mathbb{C}}\Big|_{\hat{\mathbb{r}}\to\infty}\to\hat{\mathbb{C}}_{\infty}. \tag{23}$$

The terminology for radiative heat transport can be estimated via Rosseland approximation [37], which is given as follows:

$$\hat{\mathbb{q}}_{\hat{\mathbb{r}}}=-\frac{4\hat{\alpha}_c}{3\hat{\delta}_c}\frac{\partial\hat{\mathscr{T}}^4}{\partial\hat{\mathbb{r}}}=-\frac{16\hat{\alpha}_c}{3\hat{\delta}_c}\left(\hat{\mathscr{T}}^3\frac{\partial\hat{\mathscr{T}}}{\partial\hat{\mathbb{r}}}\right), \tag{24}$$

where, $\hat{\alpha}_c$ signifies the Stefan–Boltzmann constant, while, the coefficient for mean absorption is characterized by $\hat{\delta}_c$. Therefore, by making use of Equation (24), the energy equation (Equation (21)) can be put into the following form:

$$\left(\hat{\rho}\hat{C}_p\right)_{hnf}\left(\frac{\partial\hat{\mathscr{T}}}{\partial\hat{\mathbb{r}}}\hat{\mathbb{V}}+\frac{\hat{\mathbb{R}}}{\Lambda}\frac{\partial\hat{\mathscr{T}}}{\partial\hat{\mathbb{s}}}\hat{\mathbb{U}}\right)+\frac{1}{\Lambda}\frac{\partial}{\partial\hat{\mathbb{r}}}\left(-\frac{16\hat{\alpha}}{3\hat{\delta}}\Lambda\left(\hat{\mathscr{T}}^3\frac{\partial\hat{\mathscr{T}}}{\partial\hat{\mathbb{r}}}\right)\right)=\frac{\hat{\mathbb{K}}_{hnf}}{\Lambda}\left[\left(\frac{\partial\hat{\mathscr{T}}}{\partial\hat{\mathbb{r}}}+\Lambda\frac{\partial^2\hat{\mathscr{T}}}{\partial\hat{\mathbb{r}}^2}\right)\right]. \tag{25}$$

Now, by considering the following similarity variables:

$$\hat{\mathbb{U}}=\hat{a}_1\hat{\mathbb{s}}\hat{\mathscr{F}}'(\varsigma),\ \ \acute{v}=-\frac{\hat{\mathbb{R}}}{\Lambda}\left(\hat{v}_f\hat{a}_1\right)^{0.5}\hat{\mathscr{F}}(\varsigma),\ \ \varsigma=\hat{\mathbb{r}}\left(\frac{\hat{a}_1}{\hat{v}_f}\right)^{0.5},\ \ \hat{\mathbb{P}}=\frac{\hat{\rho}_{hnf}}{\left(\hat{a}_1\hat{\mathbb{s}}\right)^{-4/2}}\hat{\mathscr{P}}(\varsigma),$$

$$\hat{\mathscr{T}}=\hat{\mathscr{T}}_{\infty}\left(1-\hat{\beta}(\varsigma)\left(1-\hat{\vartheta}_w\right)\right),\ \ \hat{\mathbb{C}}=\hat{\Theta}(\varsigma)\hat{\mathbb{C}}_w-\left(\hat{\Theta}(\varsigma)-1\right)\hat{\mathbb{C}}_{\infty}. \tag{26}$$

The equation for mass conservation (Equation (18)) is automatically verified; however, the Equations (19), (20), (22) and (25), can be written, in the dimensionless form, as:

$$\frac{\partial\hat{\mathscr{P}}}{\partial\varsigma}=\frac{\hat{\mathscr{F}}'^2}{\varsigma+\kappa_1}, \tag{27}$$

$$\frac{2\kappa_1}{\varsigma+\kappa_1}\hat{\mathscr{P}}=\frac{\hat{v}_{hnf}}{\hat{v}_f}\left[\hat{\mathscr{F}}'''+\frac{\hat{\mathscr{F}}''}{\varsigma+\kappa_1}-\frac{\hat{\mathscr{F}}'}{\left(\varsigma+\kappa_1\right)^2}\right]-\frac{\kappa_1}{\varsigma+\kappa_1}\hat{\mathscr{F}}'^2+\frac{\kappa_1}{\varsigma+\kappa_1}\hat{\mathscr{F}}\hat{\mathscr{F}}''+\frac{\kappa_1}{\left(\varsigma+\kappa_1\right)^2}\hat{\mathscr{F}}\hat{\mathscr{F}}'-\mathscr{M}\frac{\hat{\sigma}_{hnf}}{\hat{\sigma}_f}\hat{\mathscr{F}}', \tag{28}$$

$$\left(\frac{\hat{\mathbb{K}}_{hnf}}{\hat{\mathbb{K}}_f}+\mathscr{R}d\left(1+\hat{\beta}\left(\hat{\vartheta}_w-1\right)\right)^3\right)\left(\hat{\beta}''+\frac{\hat{\beta}'}{\varsigma+\kappa_1}\right)+3\mathscr{R}d\left(1+\hat{\beta}\left(\hat{\vartheta}_w-1\right)\right)^2\left(\hat{\vartheta}_w-1\right)\hat{\beta}'+\mathscr{P}r\left(\hat{\Upsilon}_3\frac{\kappa_1}{\varsigma+\kappa_1}\hat{\mathscr{F}}\hat{\beta}'\right)=0, \tag{29}$$

$$\left(\hat{\Theta}''+\frac{\hat{\Theta}'}{\varsigma+\kappa_1}\right)+\frac{\mathscr{S}c}{\hat{\Upsilon}_4}\left(\frac{\kappa_1}{\varsigma+\kappa_1}\hat{\mathscr{F}}\hat{\Theta}'-\gamma_1\hat{\Theta}\right)=0. \tag{30}$$

The associated boundary conditions, after the implementation of Equation (26), can be expressed by the following dimensionless form:

$$\hat{\mathscr{F}}(\varsigma)\Big|_{\varsigma=0}=0,\ \ \hat{\mathscr{F}}'(\varsigma)\Big|_{\varsigma=0}=1,\ \ \hat{\beta}(\varsigma)\Big|_{\varsigma=0}=1,\ \ \hat{\Theta}(\varsigma)\Big|_{\varsigma=0}=1,$$

$$\hat{\mathscr{F}}'(\varsigma)\Big|_{\varsigma\to\infty}=0,\ \ \hat{\mathscr{F}}''(\varsigma)\Big|_{\varsigma\to\infty}=0,\ \ \hat{\beta}(\varsigma)\Big|_{\varsigma\to\infty}=0,\ \ \hat{\Theta}(\varsigma)\Big|_{\varsigma\to\infty}=0. \tag{31}$$

The dimensionless quantities, arising in the above set of Equations (27)–(30), can be defined as:

$$\kappa_1=\hat{\mathbb{R}}\left(\frac{\hat{a}_1}{\hat{v}_f}\right)^{0.5},\ \mathscr{M}=\frac{\hat{\sigma}_f\hat{\mathbb{B}}_0^2}{\hat{a}_1\hat{\rho}_f},\ \mathscr{R}d=\frac{16\hat{\alpha}_c}{3\hat{\delta}_c\hat{\mathbb{K}}_f}\hat{\mathscr{T}}_{\infty}^3,\ \hat{\vartheta}_w=\frac{\hat{\mathscr{T}}_w}{\hat{\mathscr{T}}_{\infty}},\ \gamma_1=\frac{\hat{c}_0}{\hat{a}_1},\ \mathscr{S}c=\frac{\hat{v}_f}{\hat{\mathbb{D}}_f},\ \mathscr{P}r=\left(\frac{\hat{\mathbb{K}}_f}{\left(\hat{\rho}\hat{C}_p\right)_f\hat{v}_f}\right)^{-1}, \tag{32}$$

where the dimensionless radius of curvature is denoted by κ_1. $\mathscr{M}$ represents the magnetic parameter, while, the radiation and temperature ratio parameters are simultaneously symbolized by $\mathscr{R}d$ and $\hat{\vartheta}_w$.

γ_1 signifies the chemical reaction parameter. The Schmidt and Prandtl numbers are characterized by $\mathscr{S}c$ and $\mathscr{P}r$, respectively.

$$
\left.
\begin{aligned}
\hat{\Upsilon}_1 &= \frac{\hat{\mu}_f}{\hat{\mu}_{hnf}} = \frac{(1-\Phi_1)^{25/10}}{(1-\Phi_2)^{-25/10}}, \\
\hat{\Upsilon}_2 &= \frac{\hat{\rho}_{hnf}}{\hat{\rho}_f} = \left[\Phi_2\frac{\hat{\rho}_{s2}}{\hat{\rho}_f} + \left(1-\Phi_2\right)\left\{1+\left(\frac{\hat{\rho}_{s1}}{\hat{\rho}_f}-1\right)\Phi_1\right\}\right], \\
\hat{\Upsilon}_3 &= \frac{(\hat{\rho}\hat{C}_p)_{hnf}}{(\hat{\rho}\hat{C}_p)_f} = \left[\Phi_2\frac{(\hat{\rho}\hat{C}_p)_{s2}}{(\hat{\rho}\hat{C}_p)_f} + \left(1-\Phi_2\right)\left\{1+\left(\frac{(\hat{\rho}\hat{C}_p)_{s1}}{(\hat{\rho}\hat{C}_p)_f}-1\right)\Phi_1\right\}\right], \\
\hat{\Upsilon}_4 &= \frac{\hat{\mathbb{D}}_{hnf}}{\hat{\mathbb{D}}_f} = \frac{(1-\Phi_1)}{(1-\Phi_2)^{-1}}.
\end{aligned}
\right\}
\tag{33}
$$

By excluding the pressure term from Equations (27) and (28), we get

$$
\hat{\mathscr{F}}^{iv} + \frac{2\hat{\mathscr{F}}'''}{\varsigma+\kappa_1} - \frac{\hat{\mathscr{F}}''}{(\varsigma+\kappa_1)^2} + \frac{\hat{\mathscr{F}}'}{(\varsigma+\kappa_1)^3} +
\frac{\hat{\Upsilon}_1}{(\hat{\Upsilon}_2)^{-1}}\left\{
\begin{aligned}
&\frac{\kappa_1}{\varsigma+\kappa_1}\left(\hat{\mathscr{F}}\hat{\mathscr{F}}''' - \hat{\mathscr{F}}'\hat{\mathscr{F}}''\right) \\
&-\frac{\kappa_1}{(\varsigma+\kappa_1)^2}\left(\hat{\mathscr{F}}'^2 - \hat{\mathscr{F}}\hat{\mathscr{F}}''\right) - \frac{\kappa_1}{(\varsigma+\kappa_1)^3}\hat{\mathscr{F}}\hat{\mathscr{F}}'
\end{aligned}
\right\} + \mathscr{M}\hat{\Upsilon}_1\frac{\hat{\sigma}_{hnf}}{\hat{\sigma}_f}\left(\hat{\mathscr{F}}'' + \frac{\hat{\mathscr{F}}'}{\varsigma+\kappa_1}\right) = 0
\tag{34}
$$

Afterwards, the pressure $\hat{\mathscr{P}}(\varsigma)$ can be evaluated from Equation (28), which is given as:

$$
\hat{\mathscr{P}}(\varsigma) = \frac{\varsigma+\kappa_1}{2\kappa_1}\left[\frac{1}{\Lambda_1}\left\{\hat{\mathscr{F}}''' + \frac{\hat{\mathscr{F}}''}{\varsigma+\kappa_1} - \frac{\hat{\mathscr{F}}'}{(\varsigma+\kappa_1)^2}\right\} - \frac{\kappa_1}{\varsigma+\kappa_1}\hat{\mathscr{F}}'^2 + \frac{\kappa_1}{\varsigma+\kappa_1}\hat{\mathscr{F}}\hat{\mathscr{F}}'' + \frac{\kappa_1}{(\varsigma+\kappa_1)^2}\hat{\mathscr{F}}\hat{\mathscr{F}}' - \mathscr{M}\frac{\hat{\sigma}_{hnf}}{\hat{\sigma}_f}\hat{\mathscr{F}}'\right].
\tag{35}
$$

The quantities that can be practically useful in many engineering and industrial situations are, surface drag coefficient $\left(\mathscr{C}_f\right)$, the local Nusselt $\left(\mathscr{N}u_{\widehat{\mathbb{S}}}\right)$ and Sherwood $\left(\mathscr{S}h_{\widehat{\mathbb{S}}}\right)$ numbers. Their respective mathematical expressions are given as:

$$
\mathscr{C}_f = \frac{\hat{\mathbb{U}}_w^{-2}}{\hat{\rho}_f}\hat{\tau}_{\widehat{\mathbb{T}}\widehat{\mathbb{S}}}, \quad \mathscr{N}u_{\widehat{\mathbb{S}}} = \frac{(\hat{\mathrm{K}}_f/\widehat{\mathbb{S}})^{-1}}{(\hat{\mathscr{T}}_w - \hat{\mathscr{T}}_\infty)}\left(\widehat{\mathbb{Q}}_{\hat{w}} + \widehat{\mathbb{Q}}_{\widehat{\mathbb{T}}}\right), \quad \mathscr{S}h_{\widehat{\mathbb{S}}} = \frac{(\hat{\mathbb{D}}_f/\widehat{\mathbb{S}})^{-1}}{(\hat{\mathbb{C}}_w - \hat{\mathbb{C}}_\infty)}\widehat{\mathbb{Q}}_{\hat{m}},
\tag{36}
$$

where the wall shear stress is symbolized by $\hat{\tau}_{\widehat{\mathbb{T}}\widehat{\mathbb{S}}}$, while $\widehat{\mathbb{Q}}_{\hat{w}}$ and $\widehat{\mathbb{Q}}_{\hat{m}}$ simultaneously represents the rate of heat and mass transports at the wall. They can be mathematically specified as:

$$
\hat{\tau}_{\widehat{\mathbb{T}}\widehat{\mathbb{S}}} = \hat{\mu}_{hnf}\left(\frac{\partial\hat{\mathbb{U}}}{\partial\widehat{\mathbb{T}}} - \frac{\hat{\mathbb{U}}}{\Lambda}\right)\Bigg|_{\widehat{\mathbb{T}}=0}, \quad \widehat{\mathbb{Q}}_{\hat{w}} = -\hat{\mathrm{K}}_{hnf}\left(\frac{\partial\hat{\mathscr{T}}}{\partial\widehat{\mathbb{T}}}\right)\Bigg|_{\widehat{\mathbb{T}}=0}, \quad \widehat{\mathbb{Q}}_{\hat{m}} = -\hat{\mathbb{D}}_{hnf}\left(\frac{\partial\hat{\mathbb{C}}}{\partial\widehat{\mathbb{T}}}\right)\Bigg|_{\widehat{\mathbb{T}}=0}.
\tag{37}
$$

By making use of Equations (26) and (31) into Equation (30), the respective dimensionless forms, for the surface drag coefficient $\left(\mathscr{C}_f\right)$, the local Nusselt $\left(\mathscr{N}u_{\widehat{\mathbb{S}}}\right)$ and Sherwood $\left(\mathscr{S}h_{\widehat{\mathbb{S}}}\right)$ numbers are:

$$
Re_{\widehat{\mathbb{S}}}^{5/10}\mathscr{C}_f = (\hat{\Upsilon}_1)^{-1}\left(\hat{\mathscr{F}}''(\varsigma) - \frac{\hat{\mathscr{F}}'(\varsigma)}{\kappa_1}\right)\Bigg|_{\varsigma=0},
\tag{38}
$$

$$
Re_{\widehat{\mathbb{S}}}^{-5/10}\mathscr{N}u_{\widehat{\mathbb{S}}} = -\left(\frac{\hat{\mathrm{K}}_{hnf}}{\hat{\mathrm{K}}_f} + \mathscr{R}d\left(1+\hat{\beta}(\varsigma)(\hat{\vartheta}_w-1)\right)^3\right)\hat{\beta}'(\varsigma)\Bigg|_{\varsigma=0},
\tag{39}
$$

$$
Re_{\widehat{\mathbb{S}}}^{-5/10}\mathscr{S}h_{\widehat{\mathbb{S}}} = -\hat{\Upsilon}_4\hat{\Theta}'(\varsigma)\Big|_{\varsigma=0}
\tag{40}
$$

where, $Re_{\hat{\mathbb{S}}} = \hat{a}_1 \hat{\mathbb{s}}^2 / \hat{v}_f$ expresses the local Reynolds number.

4. Numerical Procedure

The numerical recipe, comprising shooting method along with the Runge–Kutta–Fehlberg technique has opted, to evaluate the system of nonlinear differential equations (Equations (34), (29) and (30)) together with the auxiliary conditions (Equation (31)). At first, the shooting technique has been employed, with which the system of nonlinear differential equations (Equations (34), (29) and (30)) undergoes a conversion procedure. Thus, a first-order initial value problem has been achieved. Afterwards, the Runge–Kutta–Fehlberg technique has been taken into account, to solve the resulting initial value problem. The computational procedure has been performed via Mathematical software 'Mathematica', by considering the step size $\Delta \varsigma = 0.001$ and the convergence criteria are set up to 10^{-6}.

5. Physical Explanation of Results

This segment is designed to scrutinize the impact of various emerging parameters on the velocity and pressure distribution. The temperature, together with concentration profiles, has also been considered. For the said purpose, the graphical simulations, along with the detailed description, have been presented. The graphical pictures have been plotted for both CuO/NaAlg nanofluid and sodium alginate (NaAlg) based (Cu − CuO) hybrid nanofluid. The main emphasis is to give the comparative study related to both types (mono and hybrid) of nanofluids. In the upcoming pictures, solid lines are dedicated to the outcomes of sodium alginate (NaAlg) based (Cu − CuO) hybrid nanofluid, while the results for *CuO/NaAlg* nanofluid has been presented via dashed lines.

Figures 2–4 have been sketched for the velocity distribution, by considering the distinct values of emerging entities like the dimensionless radius of curvature κ_1, Magnetic parameter $\hat{\mathscr{M}}$ and the volume fractions for both mono and hybrid nanofluids (Φ_1 and Φ_2), respectively. From Figure 2, a definite rise in the horizontal, as well as vertical components of velocity, have been witnessed with the decreasing values of κ_1 (or increasing the dimensionless curvature). This rising behavior is more prominent, in the case of the vertical velocity as compared to the horizontal velocity. The physical reasoning behind this fact is the existence of the centrifugal force, which the fluid, over a curved stretching surface, may encounter while moving along the circular path. In actual, the curvature of the surface is mainly responsible for the production of the centrifugal force, corresponding to the centripetal acceleration, whose direction is normal to the center of curvature to maintain the circular flow of the fluid. As a result of this centrifugal force, an additional disturbance named as the secondary wave has been produced, whose resulting effects are then combined with the effects of primary wave, which is caused by the surface expansion. Since, the direction of the centrifugal force is normal to the surface, therefore, a significant impact on the vertical velocity $\hat{\mathscr{F}}(\varsigma)$ has been recorded. However, the horizontal velocity $\hat{\mathscr{F}}'(\varsigma)$ experiences a small increment. In the limiting case of infinitely large radius of curvature (i.e., $\kappa_1 \to \infty$), the curved surface turned out to be a flat surface and consequently, the centrifugal force disappears. In this situation, the net effect on the flow is due to the primary flow caused by the stretched surface alone. Moreover, it was observed that the sodium alginate (NaAlg) based (Cu − CuO) hybrid nanofluid exhibited low velocity profiles along the $\hat{\mathbb{s}}$ and $\hat{\mathbb{T}}$ direction, when compared to the CuO/NaAlg nanofluid.

The influence of Magnetic parameter $\hat{\mathscr{M}}$ on the normal along with horizontal components of velocity have been presented in Figure 3a,b. A decline in the velocity fields ($\hat{\mathscr{F}}(\varsigma)$ and $\hat{\mathscr{F}}'(\varsigma)$) for both CuO/NaAlg nanofluid and sodium alginate (NaAlg) based hybrid (Cu − CuO) nanofluid has been perceived, with the growing values of the magnetic parameter $\hat{\mathscr{M}}$. The cause behind is the development of the Lorentz forces, due to the applied magnetic field, inside an electrically conducting fluid. These forces act like a resistive force, which in turn suppresses the bulk motion of the fluid and hence, the velocity, together with the thickness of momentum boundary layer, of the fluid exhibit a declining behavior [28,38,39].
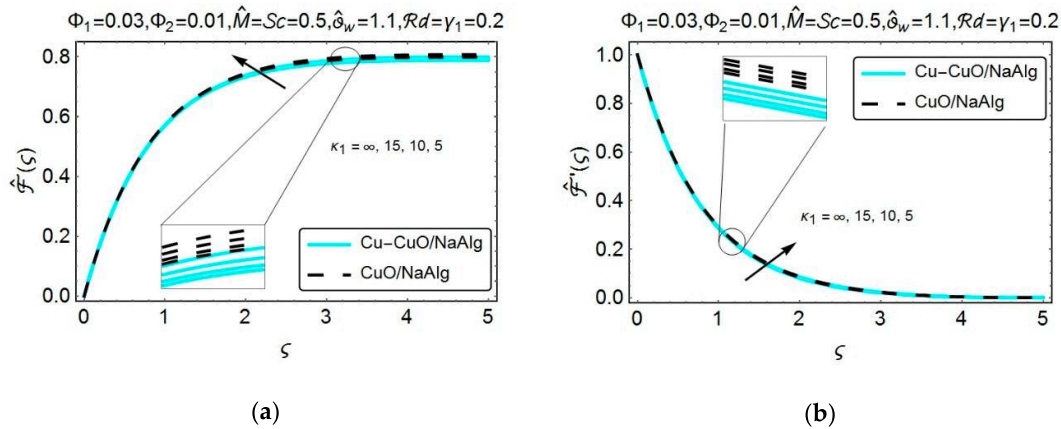
(**a**) (**b**)

Figure 2. Graphical illustration of (**a**) $\hat{\mathscr{F}}(\varsigma)$ and (**b**) $\hat{\mathscr{F}}\prime(\varsigma)$, for copious values of κ_1.

(**a**) (**b**)
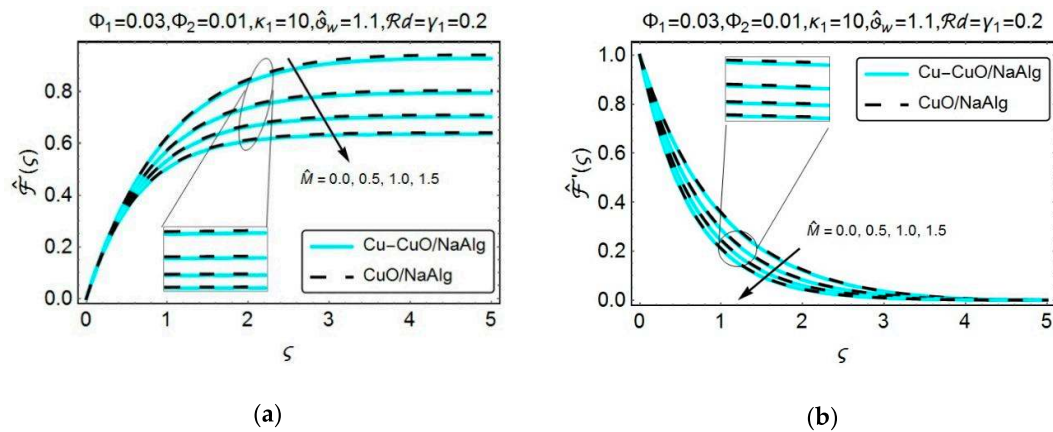
Figure 3. Graphical illustration of (**a**) $\hat{\mathscr{F}}(\varsigma)$ and (**b**) $\hat{\mathscr{F}}\prime(\varsigma)$, for copious values of $\hat{\mathscr{M}}$.

(**a**) (**b**)
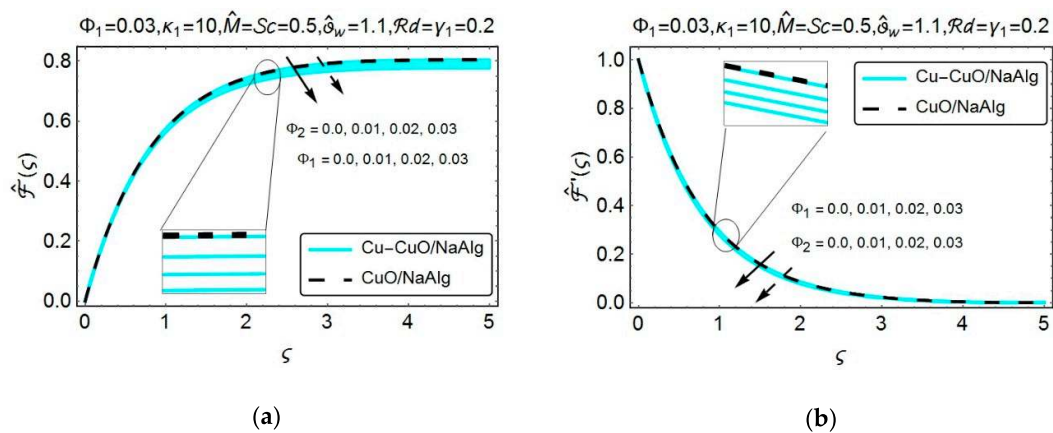
Figure 4. Graphical illustration of (**a**) $\hat{\mathscr{F}}(\varsigma)$ and (**b**) $\hat{\mathscr{F}}\prime(\varsigma)$, for copious values of Φ_1 and Φ_2.

Figure 4a,b has been designed to see the performance of nanoparticles volume fractions (Φ_1 and Φ_2) on the velocity profiles ($\hat{\mathscr{F}}(\varsigma)$ and $\hat{\mathscr{F}}\prime(\varsigma)$), respectively. Both the velocity modules, $\hat{\mathscr{F}}(\varsigma)$ and $\hat{\mathscr{F}}\prime(\varsigma)$, shows a declinatory mechanism with the increasing values of volume fractions (Φ_1 and Φ_2), for both CuO/NaAlg nanofluid and sodium alginate $(NaAlg)$ based $(Cu-CuO)$ hybrid nanofluid. In actual, the augmentation in the nanocomposites volumetric fractions mainly is responsible for the production of viscous effects within the fluid. These effects provide resistance for the further movement of the

fluid and as a result, decreases the velocity of the fluid. This particular phenomenon has been detected for both CuO/NaAlg nanofluid and sodium alginate (NaAlg) based (Cu − CuO) hybrid nanofluid. Moreover, it has been noticed that the CuO/NaAlg nanofluid has been least affected by the inclusion of nanocomposites volumetric fractions as compared to sodium alginate (NaAlg) based (Cu − CuO) hybrid nanofluid, which is due to the lower density values of the CuO/NaAlg nanofluid.

Figures 5–9 have been designed to visualize the impact of various meaningful emerging entities like the dimensionless radius of curvature κ_1, Magnetic parameter $\hat{\mathcal{M}}$, the volume fractions for both mono and hybrid nanofluids (Φ_1 and Φ_2), Radiation parameter $\mathcal{R}d$ and the temperature difference parameter $\hat{\vartheta}_w$ on the temperature distribution $\hat{\beta}(\varsigma)$. An upsurge in the temperature distribution $\hat{\beta}(\varsigma)$, for both CuO/NaAlg nanofluid and sodium alginate (NaAlg) based (Cu − CuO) hybrid nanofluid has been noticed with the decreasing values of κ_1 (see Figure 5). The main cause behind is the heat conduction process, which grows when the curvature is employed in the flat expanding surface. From Figure 6, one can see an increment in the temperature behavior with the growing values of magnetic parameter $\hat{\mathcal{M}}$. The applied magnetic field develops the Lorentz forces within the fluid, which behaves like a resistive force and eventually the friction effects have been recorded inside the fluid. These effects ultimately produce the heat, and consequently, an intensification in the temperature profile has been achieved [28,38,39]. Moreover, it is noteworthy that the (Cu − CuO)/NaAlg hybrid nanofluid exhibits a higher temperature profile as compared to CuO/NaAlg nanofluid.
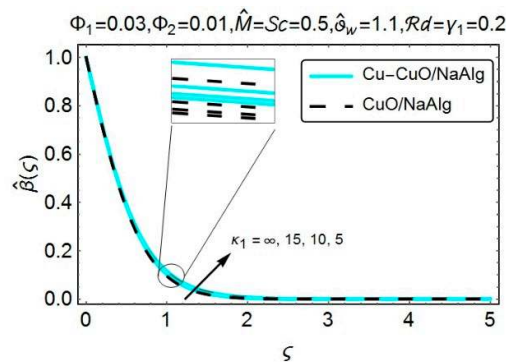

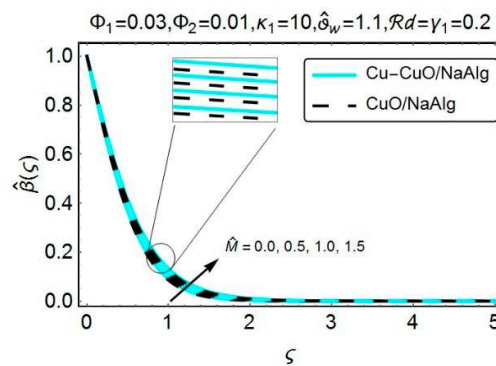**Figure 5.** Graphical illustration of $\hat{\beta}(\varsigma)$, for copious values of κ_1.

Figure 6. Graphical illustration of $\hat{\beta}(\varsigma)$, for copious values of $\hat{\mathcal{M}}$.
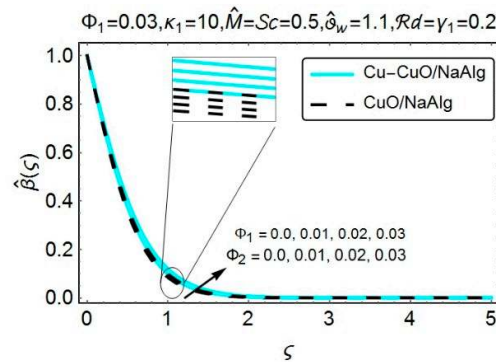
Figure 7. Graphical illustration of $\hat{\beta}(\varsigma)$, for copious values of Φ_1 and Φ_2.
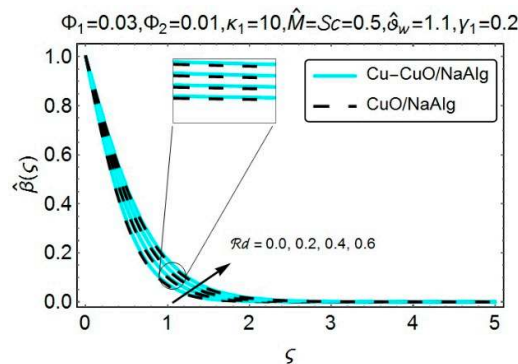
Figure 8. Graphical illustration of $\hat{\beta}(\varsigma)$, for copious values of $\mathscr{R}d$.
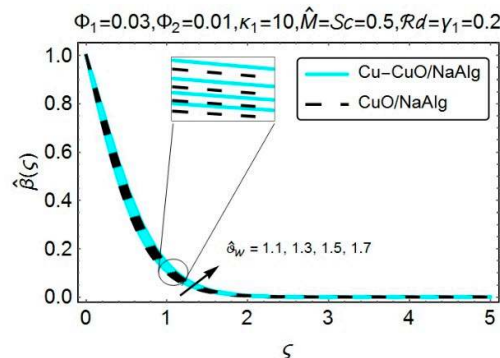

Figure 9. Graphical illustration of $\hat{\beta}(\varsigma)$, for copious values of $\hat{\vartheta}_w$.

The role of increasing nanocomposites volumetric fractions on the temperature profiles was displayed in Figure 7. It was noted that the inclusion of nano-sized structures with variable volumetric fractions contributes to the enhancement of the temperature of the fluid. The physical reasoning behind this fact is the intensification in the thermal conductive properties of the host fluid. Therefore, it is understood that the temperature gets its maximum values in the case of $(Cu-CuO)/NaAlg$ hybrid nanofluid, which can be seen from Figure 7. Figure 8 portrays the impact of the radiation parameter $\mathscr{R}d$ on the temperature profile. The increment in the radiation parameter significantly supports the augmentation in the temperature distribution. The actual reason is the drop in the mean absorption coefficient, which considerably improves the radiative effects inside the fluid and consequently, boosts the temperature of the fluid. Besides, this phenomenon has been accomplished for both CuO/NaAlg nanofluid and sodium alginate $(NaAlg)$ based $(Cu-CuO)$ hybrid nanofluid.

The effectiveness of temperature difference parameter $\hat{\vartheta}_w$ on the temperature distribution, has been offered via Figure 9. A rise in temperature, for both CuO/NaAlg nanofluid and sodium alginate $\left(\text{NaAlg}\right)$ based $\left(\text{Cu}-\text{CuO}\right)$ hybrid nanofluid has been chronicled with the growing values of $\hat{\vartheta}_w$. The augmentation in $\hat{\vartheta}_w$ greatly supports the improvement in temperature differences and hence, an enhancement in temperature has been perceived. Besides, the $\left(\text{Cu}-\text{CuO}\right)$/NaAlg hybrid nanofluid reveals the maximum temperature values.

Figures 10–14 provides the graphical simulation for the concentration profile $\hat{\Theta}(\varsigma)$, by taking the effects of various embedded entities like the dimensionless radius of curvature κ_1, magnetic parameter $\hat{\mathcal{M}}$, the volume fractions for both mono and hybrid nanofluids (Φ_1 and Φ_2), Schmidt number $\mathcal{S}c$ and the chemical reaction parameter γ_1 into consideration. It can be seen from Figure 10 that the reduction in the concentration profile $\hat{\Theta}(\varsigma)$ has been perceived with the decreasing κ_1. A drop in the dimensionless radius of curvature κ_1 supports the curvilinear nature of the surface. As the curviness of the surface increases, the kinematic viscosity decreases. So, the density along with the mass of the host fluid experiences a decline, and hence, the concentration profile reduces. The increment in the magnetic parameter $\hat{\mathcal{M}}$ significantly takes part in enhancing the concentration profile, for both CuO/NaAlg nanofluid and sodium alginate $\left(\text{NaAlg}\right)$ based $\left(\text{Cu}-\text{CuO}\right)$ hybrid nanofluid (see Figure 11). In fact, the implementation of magnetic field yields the Lorentz forces, which is responsible for the production of a significant amount of heat inside the fluid. This, in actual, slows down the process of heat and mass transfer from the wall and hence, boosts the temperature as well as the concentration profiles. The inset pictures also revealed the fact that the CuO/NaAlg nanofluid possessed maximum concentration values.
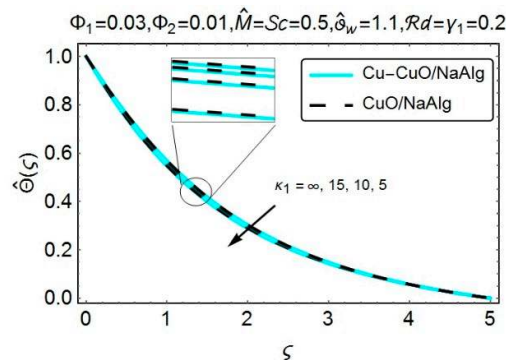

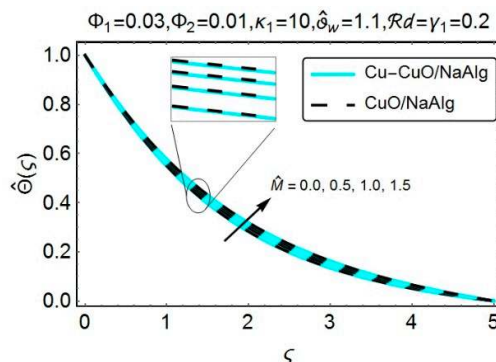**Figure 10.** Graphical illustration of $\hat{\Theta}(\varsigma)$, for copious values of κ_1.

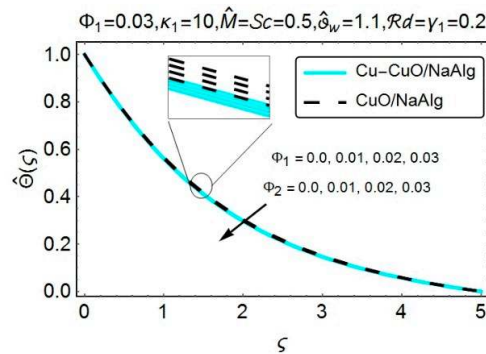**Figure 11.** Graphical illustration of $\hat{\Theta}(\varsigma)$, for copious values of $\hat{\mathcal{M}}$.

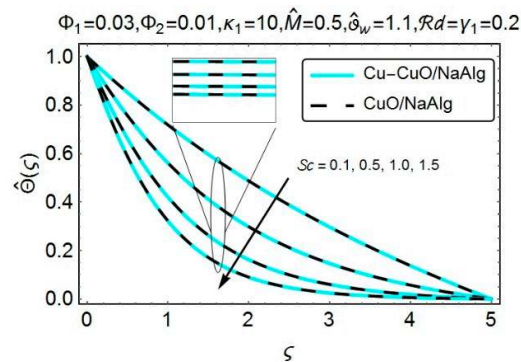**Figure 12.** Graphical illustration of $\hat{\Theta}(\varsigma)$, for copious values of Φ_1 and Φ_2.

Figure 13. Graphical illustration of $\hat{\Theta}(\varsigma)$, for copious values of $\mathscr{S}c$.
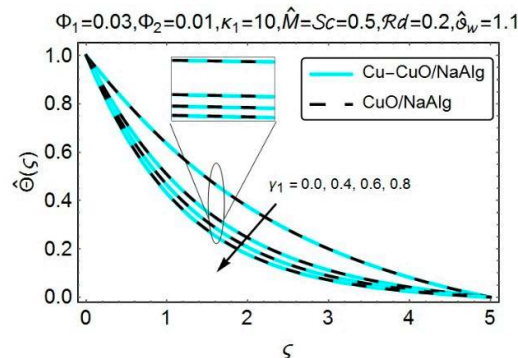

Figure 14. Graphical illustration of $\hat{\Theta}(\varsigma)$, for copious values of γ_1.

Figure 12 has been plotted to see the impact of nanocomposites volumetric fractions on the concentration profile $\hat{\Theta}(\varsigma)$. It is notable that by increasing the volumetric fraction of nano additives, the decrement in the solute concentration was perceived. Besides, the concentration profile possessed lower values for sodium alginate (NaAlg) based $(\text{Cu} - \text{CuO})$ hybrid nanofluid. The impact of Schmidt number $\mathscr{S}c$ on the concentration profile, for both CuO/NaAlg nanofluid and sodium alginate (NaAlg) based $(\text{Cu} - \text{CuO})$ hybrid nanofluid has been depicted in Figure 13. The higher estimated values of Schmidt number $\mathscr{S}c$ considerably lessened the concentration of the species. As $\mathscr{S}c$ indicates the ratio of viscous diffusion rate and the mass diffusion rate. Thus, for growing values of $\mathscr{S}c$, the rate of mass diffusion decayed, and hence the concentration field endured an absolute decline.

Figure 14 has been offered to display the influence of chemical reaction parameter γ_1 on the concentration field $\hat{\Theta}(\varsigma)$. It is notable that the growing values of chemical reaction parameter γ_1 significantly reduced the concentration profile $\hat{\Theta}(\varsigma)$. The physical explanation of this behavior is

that the increment in γ_1 implies the destructive chemical reaction at a higher rate, which, in turn, effectively dissolves or terminates the liquid species. Hence, a decay in the concentration profile, for both CuO/NaAlg nanofluid and sodium alginate (NaAlg) based (Cu – CuO) hybrid nanofluid was accomplished.

Figures 15–17 have been designed to inspect the behavior of pressure profile under the impact of the dimensionless radius of curvature κ_1, magnetic parameter $\hat{\mathcal{M}}$, the volume fractions for both mono and hybrid nanofluids (Φ_1 and Φ_2). Figure 15 demonstrates the impact of the dimensionless radius of curvature κ_1 on the pressure distribution. A drop in the dimensionless radius of curvature κ_1, means that the curviness of the surface increases, which significantly supported the growing absolute values of pressure and this phenomenon was quite prominent inside the boundary layer. However, the effectiveness of the pressure profile seemed to be negligible as we moved away from the curved surface. The physical aspect behind this behavior was that as the distance from the surface increased, the streamlines, for both CuO/NaAlg nanofluid and sodium alginate (NaAlg) based (Cu – CuO) hybrid nanofluid, acted in the same way as they could be noticed in the case of flat dilating surface. In the limiting case of an infinitely large radius of curvature (i.e., $\kappa_1 \to \infty$), which corresponds to the flat stretching surface, consistent behavior of the pressure was recorded not only inside but also the outside of the boundary layer. However, in the case of a stretchable curved surface, the effectiveness of pressure could not be ignored, as it proved its dominancy inside the boundary layer. Figure 16 provides the pictorial view of the pressure profile due to the varying value of the magnetic parameter $\hat{\mathcal{M}}$. It is noteworthy that, at the initial stage, the absolute values of the pressure distribution exhibited a declining behavior with the growing values of the magnetic parameter. However, reversed behavior was perceived after $\varsigma = 1$. The same behavior was recorded for the varying values of the dimensionless radius of curvature κ_1. As the curviness was introduced in the surface, the pressure did not show a consistent behavior inside and outside the boundary layer. Moreover, the inset pictures (from Figures 15 and 16) revealed the fact that, in the case of CuO/NaAlg nanofluid, the pressure distribution exhibited a dominating behavior, outside the boundary layer, as compared to the sodium alginate (NaAlg) based (Cu – CuO) hybrid nanofluid.
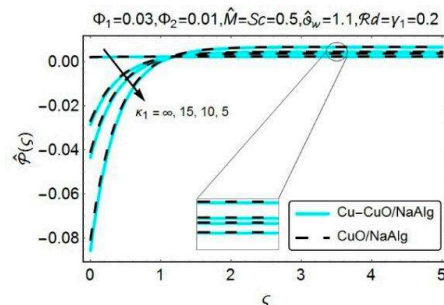

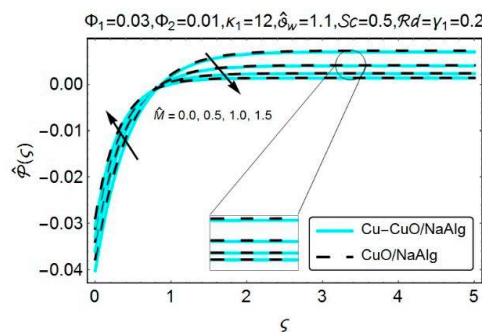**Figure 15.** Graphical illustration of $\hat{\mathscr{P}}(\varsigma)$, for copious values of κ_1.

Figure 16. Graphical illustration of $\hat{\mathscr{P}}(\varsigma)$, for copious values of $\hat{\mathcal{M}}$.
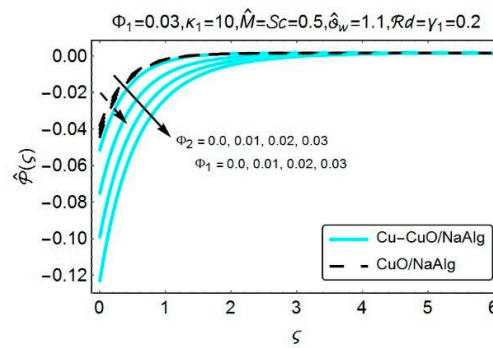
Figure 17. Graphical illustration of $\hat{\mathscr{P}}(\varsigma)$, for copious values of Φ_1 and Φ_2.

Figure 17 elucidates the impact of volumetric fraction of nano-sized structures (Φ_1 and Φ_2) on the pressure profile. The plot was designed for both CuO/NaAlg nanofluid and sodium alginate (NaAlg) based (Cu − CuO) hybrid nanofluid. The increasing nanocomposites volumetric fractions (Φ_1 and Φ_2), successfully contributed to the growing absolute values for the pressure profile. Moreover, the CuO/NaAlg nanofluid presented the lower absolute values of pressure profile, inside the boundary layer, when compared to (Cu − CuO)/NaAlg hybrid nanofluid.

Figures 18 and 19 have been painted to visualize the consequences of various meaningful emerging variables like the dimensionless radius of curvature κ_1, magnetic parameter $\hat{\mathscr{M}}$, the volume fractions for both mono and hybrid nanofluids (Φ_1 and Φ_2) on the coefficient of skin friction drag. It can be elucidated from Figure 18 that the coefficient for skin friction, for both CuO/NaAlg nanofluid and sodium alginate (NaAlg) based (Cu − CuO) hybrid nanofluid, experienced a decline with the growing values of the dimensionless radius of curvature κ_1. This means that the surface drag force needs to be intensified when the curviness has been employed in the flat stretching surface. On the contrary, the magnetic parameter $\hat{\mathscr{M}}$ displayed a reversed behavior and the surface drag force exhibits an increment with the growing values of magnetic parameter $\hat{\mathscr{M}}$. The inclusion of nanometer-sized structures within the fluid also displayed an improvement in the surface drag force, and this can be observed for both mono and hybrid nanofluids (see Figure 19). Moreover, it was evident from both Figures 18 and 19 that the surface drag force, in the case of (Cu − CuO)/NaAlg hybrid nanofluid, displayed its dominancy when compared to the CuO/NaAlg nanofluid.
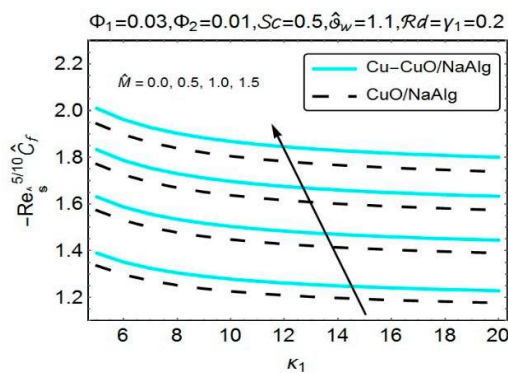

Figure 18. Graphical illustration of surface drag coefficient, for copious values of $\hat{\mathscr{M}}$.
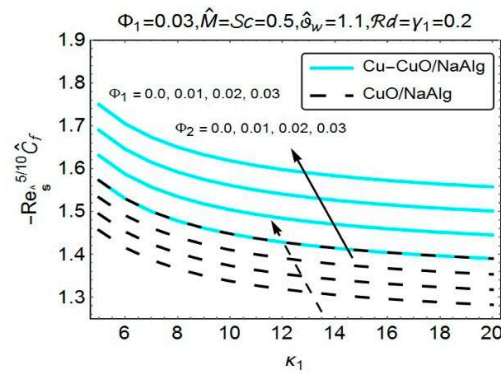
Figure 19. Graphical illustration of surface drag coefficient, for copious values of Φ_1 and Φ_2.

In order to assess the behavior of the local rate of heat transfer, due to varying values of the dimensionless radius of curvature κ_1, magnetic parameter $\hat{\mathscr{M}}$, the volume fractions for both mono and hybrid nanofluids (Φ_1 and Φ_2), radiation parameter $\mathscr{R}d$ and the temperature difference parameter $\hat{\vartheta}_w$. Figures 20–22 has been painted. The rate with which heat transfers, from the surface of the curved sheet, exhibited a declinatory behavior, as the curviness of the surface tended to the flatness of the surface (see Figure 20), and this behavior was recorded for both mono and hybrid nanofluids. It means that the rate, with which surface's heat transmits, seems to be quite prominent in the case of the curved stretching surface. Besides, from Figure 20, the heat transfer rate displays a similar declining behavior with the increasing magnetic variable $\hat{\mathscr{M}}$. Since the development of Lorentz forces, due to externally applied magnetic field, generates the friction effects inside the fluid, which in turn raises the temperature of the fluid and hence, slows down the process of transferring the heat from the surface. The inclusion of nanometer-sized structures (Φ_1 and Φ_2), with different volume fractions, plays a vital role in enhancing the heat transfer rate, and it can be easily figured out from Figure 21. Physically, the addition of nanometer-sized particles enriches the thermal properties of the host fluid, and as a result, the improvement in the heat-conducting properties is quite obvious. Moreover, the heat flux rate shows its proficiency in the case of $(\text{Cu} - \text{CuO})/\text{NaAlg}$ hybrid nanofluid, which was mainly due to the existence of higher thermal conducting values as compared to CuO/NaAlg nanofluid.

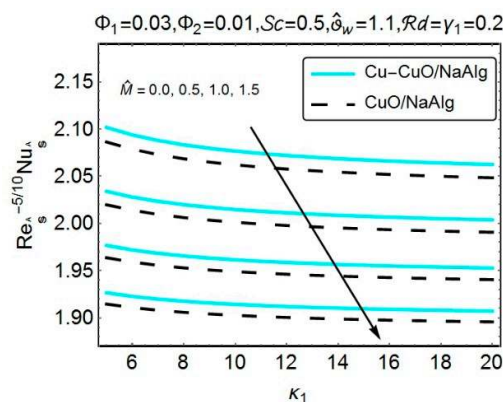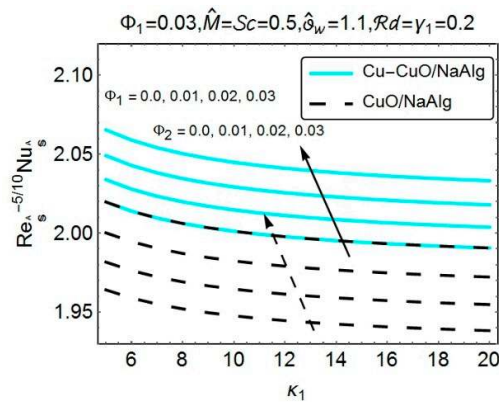**Figure 20.** Graphical illustration of heat transport rate, for copious values of $\hat{\mathscr{M}}$.

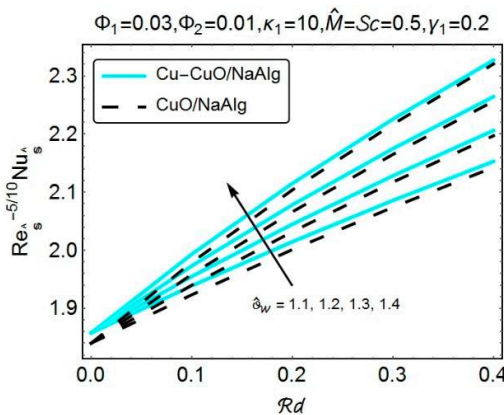**Figure 21.** Graphical illustration of heat transport rate, for copious values of Φ_1 and Φ_2.

Figure 22. Graphical illustration of heat transport rate, for copious values of $\hat{\vartheta}_w$.

Figure 22 highlights the effects of radiative variable $\mathscr{R}d$ and the temperature difference variable $\hat{\vartheta}_w$ on the local rate of heat flux and the results were calculated, by considering both mono and hybrid nanofluids. The figure provided evidence that the radiative variable $\mathscr{R}d$ played a vital role in extensively transferring the heat from the system. The temperature difference variable $\hat{\vartheta}_w$ also supported the process of heat flux, and this behavior was observed for both mono and hybrid nanofluids. Furthermore, the CuO/NaAlg nanofluid depicted a lower heat transfer rate as compared to the (Cu − CuO)/NaAlg hybrid nanofluid.

Figures 23–25 have been designed to see the impact of the dimensionless radius of curvature κ_1, magnetic parameter $\hat{\mathscr{M}}$, the volume fractions for both mono and hybrid nanofluids (Φ_1 and Φ_2), Schmidt number $\mathscr{S}c$ and the chemical reaction parameter γ_1, on the local rate of mass transfer. A declinatory behavior has been perceived for the local rate of heat transfer, with the growing values of the dimensionless radius of curvature κ_1 (see Figure 23). This behavior was noted for both mono and hybrid nanofluids. Thus, it could be concluded that the rate, with which mass transfers, exhibited its dominancy in the case of a stretchable curved surface. The mass transferring rate behaved in a decreasing manner with the increasing magnetic variable $\hat{\mathscr{M}}$. The magnetic field was responsible for the development of the Lorentz forces, which could extensively heat up the fluid. As a result, the temperature, along with the concentration profiles, increased, and thus the process of mass transfer decreased. The dispersion of nanometer-sized particles (Φ_1 and Φ_2), with variable volume fractions, could certainly take part in slowing down the mass transferring process, and this could be easily detected from Figure 24. Moreover, the CuO/NaAlg nanofluid illustrates an increment in the process of mass transfer, as compared to the (Cu − CuO)/NaAlg hybrid nanofluid.
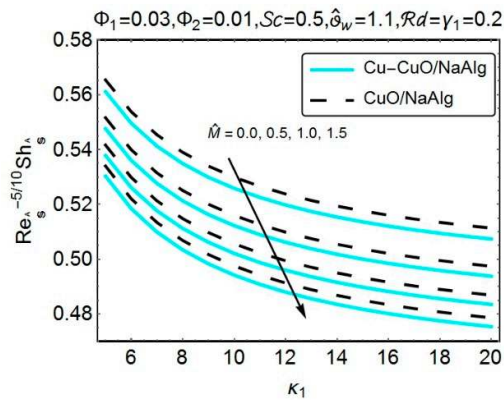
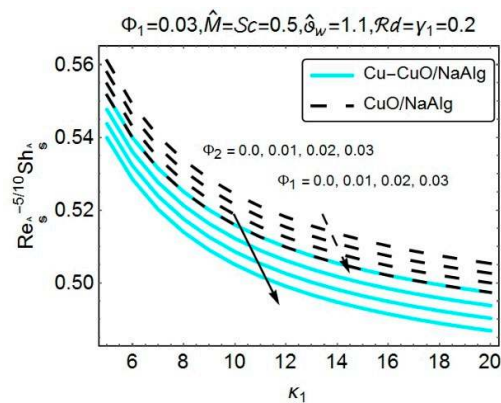**Figure 23.** Graphical illustration of the mass transport rate, for copious values of $\hat{\mathscr{M}}$.

Figure 24. Graphical illustration of the mass transport rate, for copious values of Φ_1 and Φ_2.
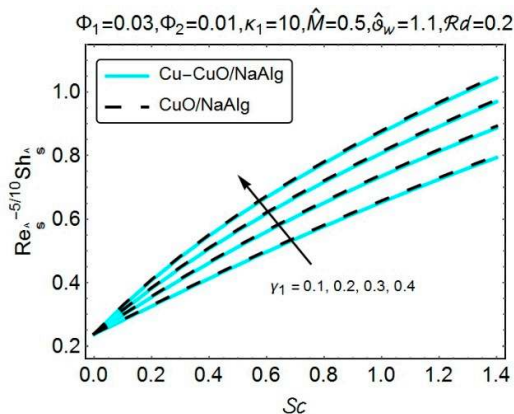
Figure 25. Graphical illustration of the mass transport rate, for copious values of γ_1.

Figure 25 has been painted to assess the influence of Schmidt number $\mathscr{S}c$ and the chemical reaction parameter γ_1, on the local rate of mass transfer. It can be noticeable that the mass transferring process has been significantly improved, with the growing values of Schmidt number $\mathscr{S}c$. Almost a similar behavior has been detected with the increasing values of chemical reaction variable γ_1. Moreover, the improvement in the rate of mass transfer was recorded for CuO/NaAlg nanofluid as well as the $\left(\text{Cu}-\text{CuO}\right)$/NaAlg hybrid nanofluid.

To validate the existence of numerical procedure, a comparison of the numerical results, for the surface drag coefficient $\left(-Re_{\hat{\mathbb{S}}}^{5/10}\hat{\mathscr{C}}_f\right)$, with the previously existing outcomes of [24,26,39], [24] has been

presented in Table 2. A good match, among the outcomes, can be visible from the table for varying values of dimensionless radius of curvature κ_1 and magnetic parameter $\hat{\mathscr{M}}$.

Table 2. Comparison of the numerical results for the surface drag coefficient $\left(-Re_{\hat{\mathbb{S}}}^{5/10}\hat{\mathscr{C}}_f\right)$, by assuming $\Phi_1 = \Phi_2 = 0$.

κ_1	$\widehat{\mathcal{M}}$	Abbas et al. [39]	Xu and Lee [24]	Mabood and Das [26]	Present Results
5	0.0	1.15763	-	-	1.1576312
10		1.07349	-	-	1.0734886
50		1.01405	-	-	1.0140492
100		1.00704	-	-	1.0070384
1000		1.00079	-	-	1.0007993
∞		1.00000	-	-	1.0000000
	1.0	-	1.41421	1.4142135	1.4142135
	5.0	-	2.4494	2.4494897	2.4494897
	10	-	3.3166	3.3166247	3.3166247
	50	-	7.1414	7.1414284	7.1414284
	100	-	10.0498	10.049875	10.049875
	1000	-	-	31.638584	31.638584

6. Conclusions

Flow of $(Cu-CuO)/NaAlg$ hybrid nanofluid, under the action of an externally applied magnetic field, over a curved expanding surface were investigated. By taking the effects of thermal radiation and the chemical reaction into consideration, the temperature, along with concentration distribution, was also critically examined. The following were the major findings of this study:

- Radial, as well as horizontal velocity components, boosted with decreasing dimensionless radius of curvature κ_1, while a declinatory behavior was perceived via increasing magnetic parameter $\hat{\mathscr{M}}$, and nano additives volumetric fractions Φ_1/Φ_2.
- The sodium alginate $(NaAlg)$ based $(Cu-CuO)$ hybrid nanofluid exhibited low-velocity profiles along the $\hat{\mathbb{s}}$ and $\hat{\mathbb{r}}$ direction, when compared to the CuO/NaAlg nanofluid.
- Temperature elevation was chronicled for the increasing values of dimensionless radius of curvature κ_1, magnetic parameter $\hat{\mathscr{M}}$, nano additives volumetric fractions Φ_1/Φ_2, radiation parameter $\mathscr{R}d$ and temperature difference parameter $\hat{\vartheta}_w$ and in all cases, the $(Cu-CuO)/NaAlg$ hybrid nanofluid revealed the maximum temperature values.
- An improvement in the concentration profile was noticed with increasing magnetic parameter $\hat{\mathscr{M}}$. However, a reversed behavior was recorded for rising values of nano additives volumetric fractions Φ_1/Φ_2, Schmidt number $\mathscr{S}c$ and chemical reaction parameter γ_1.
- The surface drag force was higher for magnetic parameter $\hat{\mathscr{M}}$, while it decayed through increasing dimensionless radius of curvature κ_1, and nano additives volumetric fractions Φ_1/Φ_2.
- Elevation in nanoadditives volumetric fractions Φ_1/Φ_2, radiation parameter $\mathscr{R}d$ and temperature difference parameter $\hat{\vartheta}_w$ supported the higher transferring of heat; however, an opposite behavior was noticed via increasing dimensionless radius of curvature κ_1 and magnetic parameter $\hat{\mathscr{M}}$.
- The heat flux rate showed its proficiency in the case of $(Cu-CuO)/NaAlg$ hybrid nanofluid as compared to CuO/NaAlg nanofluid.
- Sherwood number, for $(Cu-CuO)/NaAlg$ hybrid nanofluid decayed for the dimensionless radius of curvature κ_1, magnetic parameter $\hat{\mathscr{M}}$ and nano additives volumetric fractions Φ_1/Φ_2, while it boosted via Schmidt number $\mathscr{S}c$ and chemical reaction parameter γ_1.

The present investigations had tremendous practical relevance, especially in the polymer and chemical industries, where the high-quality polymer sheets were designed via rapid expansion processes. Moreover, the estimated results would hopefully provide the basis for the study of the

blood flowing through arteries. The aspect of assuming these arteries (either straight tube-shaped or curved tube-shaped) as flexible and being stretchable, further opens the new area of research.

Author Contributions: Conceptualization, U.K. and I.K.; Investigation, F.S. and E.-S.M.S.; Methodology, N.A.; Supervision, S.T.M.-D.

Conflicts of Interest: The authors declare no conflict of interest.

Nomenclature

$\hat{a}_1$	Stretching rate of the surface at $\hat{\mathbb{r}} = \hat{\mathbb{R}}$, $\left(\text{s}^{-1}\right)$
$\hat{c}_0$	Chemical reaction
$\hat{\mathbb{R}}$	Radius of curvature, (m)
$\hat{\mathbb{B}}_0$	Magnetic field strength
$\hat{\mathbb{K}}$	Thermal conductivity, $\left(\text{Wm}^{-1}\text{K}^{-1}\right)$
$\hat{\mathbb{D}}$	Mass diffusivity, m^2s^{-1}
$\hat{\mathbb{P}}$	Dimensional pressure, $\left(\text{N m}^{-2}\right)$
$\hat{\mathscr{T}}$	Temperature, (K)
$\hat{\mathbb{C}}$	Concentration
$\hat{\mathbb{U}}, \hat{\mathbb{V}}$	Velocity component along $\hat{\mathbb{s}}$ and $\hat{\mathbb{r}}$ directions, respectively, $\left(\text{m s}^{-1}\right)$

Dimensionless Parameters

$\mathscr{P}r$	Prandtl number
$\hat{\mathscr{C}}_f$	Surface drag coefficient
$\mathscr{N}u_{\hat{\mathbb{s}}}$	Local Nusselt number
$\mathscr{S}h_{\hat{\mathbb{s}}}$	Local Sherwood number
$\mathscr{S}c$	Schmidt number
$\mathscr{R}d$	Radiation parameter
$Re_{\hat{\mathbb{s}}}$	Local Reynolds number
γ_1	Chemical reaction parameter
$\hat{\mathscr{M}}$	Magnetic parameter
κ_1	Dimensionless radius of curvature
$\hat{\vartheta}_w$	Temperature ratio parameter

Greek Symbols

$\hat{\alpha}_c$	Stefan–Boltzmann constant
$\hat{\delta}_c$	Coefficient for mean absorption
ς	Similarity variable
$\hat{\tau}_{\hat{\mathbb{r}}\hat{\mathbb{s}}}$	Shear stress, $\left(\text{N m}^{-2}\right)$
$\hat{\sigma}$	Electrical conductivity
$\hat{\nu}$	Kinematic viscosity, $\left(\text{m}^2\text{s}^{-1}\right)$
$\hat{\rho}$	Density, $\left(\text{kgm}^{-3}\right)$
$\hat{\mu}$	Dynamic viscosity, $\left(\text{N.s m}^{-2}\right)$
$\left(\hat{\rho}\hat{C}_p\right)$	Specific heat capacity, $\left(\text{J K}^{-1}\right)$
Φ_1	Solid volume fraction of CuO nano additives
Φ_2	Solid volume fraction of Cu nano additives

Subscripts

hnf	Hybrid nanofluid
nf	Regular nanofluid
f	Host fluid (Sodium alginate)

| $s1$ | Solid nano additives of *CuO* |
| $s2$ | Solid nano additives of *Cu* |

Abbreviations

NaAlg	Sodium alginate
H_2O	Water
CuO	Copper Oxide
Cu	Copper
RKF	Runge–Kutta–Fehlberg Method

References

1. Özerinç, S.; Kakaç, S.; YazIcIoⓔlu, A.G. Enhanced thermal conductivity of nanofluids: A state-of-the-art review. *Microfluid. Nanofluidics* **2010**, *8*, 145–170. [CrossRef]

2. Choi, S.U.S. Enhancing thermal conductivity of fluids with nanoparticles. In *Developments and Applications of Non-Newtonian Flows*; Singer, D.A., Wang, H.P., Eds.; ASME: New York, NY, USA, 1995; pp. 99–106.

3. Choi, S.U.S.; Zhang, Z.G.; Yu, W.; Lockwood, F.E.; Grulke, E.A. Anomalous thermal conductivity enhancement in nanotube suspensions. *Appl. Phys. Lett.* **2001**, *79*, 2252–2254. [CrossRef]

4. Maxwell, J.C. *Electricity Amd Magnetism*, 3rd ed.; Clarendon: Oxford, UK, 1904.

5. Bruggeman, D.A.G. Berechnzcrrg verschCedcner physikalducher Eonstanten von heterogenew Yuhstan.xen 1. *Ann. Phys.* **1935**, *416*, 636–664. [CrossRef]

6. Hamilton, R.L.; Crosser, O.K. Thermal Conductivity of Heterogeneous Two-Component Systems. *Ind. Eng. Chem. Fundam.* **1962**, *1*, 187–191. [CrossRef]

7. Pak, B.C.; Cho, Y.I. Hydrodynamic and heat transfer study of dispersed fluids with submicron metallic oxide particles. *Exp. Heat Transf.* **1998**, *11*, 151–170. [CrossRef]

8. Mamut, E. Characterization of heat and mass transfer properties of nanofluids. *Rom. J. Phys.* **2006**, *51*, 5–12.

9. Hayat, T.; Nawaz, S.; Alsaedi, A.; Rafiq, M. Mixed Convective Peristaltic Flow of Water Based Nanofluids with Joule Heating and Convective Boundary Conditions. *PLoS ONE* **2016**, *11*, e0153537. [CrossRef]

10. Hakeem, A.A.; Saranya, S.; Ganga, B. Comparative study on Newtonian/non-Newtonian base fluids with magnetic/non-magnetic nanoparticles over a flat plate with uniform heat flux. *J. Mol. Liq.* **2017**, *230*, 445–452. [CrossRef]

11. Brinkman, H.C. The viscosity of concentrated suspensions and solutions. *J. Chem. Phys.* **1952**, *20*, 571. [CrossRef]

12. Devi, S.P.A.; Devi, S.S.U. Numerical investigation of hydromagnetic hybrid Cu-Al2O3/water nanofluid flow over a permeable stretching sheet with suction. *Int. J. Nonlinear Sci. Numer. Simul.* **2016**, *17*, 249–257. [CrossRef]

13. Ranga Babu, J.A.; Kumar, K.K.; Srinivasa Rao, S. State-of-art review on hybrid nanofluids. *Renew. Sustain. Energy Rev.* **2017**, *77*, 551–565. [CrossRef]

14. Niihara, K. New Design Concept of Structural Ceramics. *J. Ceram. Soc. Jpn.* **1991**, *99*, 974–982. [CrossRef]

15. Jana, S.; Salehi-Khojin, A.; Zhong, W.-H. Enhancement of fluid thermal conductivity by the addition of single and hybrid nano-additives. *Thermochim. Acta* **2007**, *462*, 45–55. [CrossRef]

16. Suresh, S.; Venkitaraj, K.P.; Selvakumar, P.; Chandrasekar, M. Synthesis of Al2O3-Cu/water hybrid nanofluids using two step method and its thermo physical properties. *Colloids Surf. A Physicochem. Eng. Asp.* **2011**, *388*, 41–48. [CrossRef]

17. Suresh, S.; Venkitaraj, K.P.; Selvakumar, P.; Chandrasekar, M. Effect of Al2O3–Cu/water hybrid nanofluid in heat transfer. *Exp. Therm. Fluid Sci.* **2012**, *38*, 54–60. [CrossRef]

18. Balla, H.H.; Abdullah, S.; MohdFaizal, W.; Zulkifli, R.; Sopian, K. Numerical Study of the Enhancement of Heat Transfer for Hybrid CuO-Cu Nanofluids Flowing in a Circular Pipe. *J. Oleo Sci.* **2013**, *62*, 533–539. [CrossRef]

19. Saba, F.; Ahmed, N.; Khan, U.; Waheed, A.; Rafiq, M.; Mohyud-Din, S.T. Thermophysical Analysis of Water Based (Cu–Al2O3) Hybrid Nanofluid in an Asymmetric Channel with Dilating/Squeezing Walls Considering Different Shapes of Nanoparticles. *Appl. Sci.* **2018**, *8*, 1549. [CrossRef]

20.　Ahmed, N.; Saba, F.; Khan, U.; Khan, I.; Alkanhal, T.A.; Faisal, I.; Mohyud-Din, S.T. Spherical shaped Ag-Fe3O4H2O Hybrid Nanofluid Flow Squeezed between Two Riga Plates with Nonlinear Thermal Radiation and Chemical Reaction Effects. *Energies* **2019**, *12*, 76. [CrossRef]

21.　Sakiadis, B.C. Boundary-layer behavior on continuous solid surfaces: I. Boundary-layer equations for two-dimensional and axisymmetric flow. *AIChE J.* **1961**, *7*, 26–28. [CrossRef]

22.　Crane, L.J. Flow past a stretching plate. *Z. Angew. Math. Phys. ZAMP* **1970**, *21*, 645–647. [CrossRef]

23.　Gupta, P.S.; Gupta, A.S. Heat and mass transfer on a stretching sheet with suction or blowing. *Can. J. Chem. Eng.* **1977**, *55*, 744–746. [CrossRef]

24.　Xu, L.; Lee, E.W.M. Variational iteration method for the magnetohydrodynamic flow over a nonlinear stretching sheet. *Abstr. Appl. Anal.* **2013**, *2013*, 1–5. [CrossRef]

25.　Bhattacharyya, K.; Uddin, M.S. Reactive Solute Diffusion in Boundary Layer Flow through a Porous Medium over a Permeable Flat Plate with Power-Law Variation in Surface Concentration. *J. Eng.* **2013**, *2013*, 1–7. [CrossRef]

26.　Mabood, F.; Das, K. Melting heat transfer on hydromagnetic flow of a nanofluid over a stretching sheet with radiation and second-order slip. *Eur. Phys. J. Plus* **2016**, *131*, 1–12. [CrossRef]

27.　Sajid, M.; Ali, N.; Javed, T.; Abbas, Z. Stretching a Curved Surface in a Viscous Fluid. *Chin. Phys. Lett.* **2010**, *27*, 024703. [CrossRef]

28.　Hayat, T.; Kiran, A.; Imtiaz, M.; Alsaedi, A. Hydromagnetic mixed convection flow of copper and silver water nanofluids due to a curved stretching sheet. *Results Phys.* **2016**, *6*, 904–910. [CrossRef]

29.　Saba, F.; Ahmed, N.; Hussain, S.; Khan, U.; Mohyud-Din, S.T.; Darus, M. Thermal Analysis of Nanofluid Flow over a Curved Stretching Surface Suspended by Carbon Nanotubes with Internal Heat Generation. *Appl. Sci.* **2018**, *8*, 395. [CrossRef]

30.　Lu, D.; Ramzan, M.; Ahmad, S.; Shafee, A.; Suleman, M. Impact of Nonlinear Thermal Radiation and Entropy Optimization Coatings with Hybrid Nanoliquid Flow Past a Curved Stretched Surface. *Coatings* **2018**, *8*, 430. [CrossRef]

31.　Reddy, M.G. Influence of Magnetohydrodynamic and Thermal Radiation Boundary Layer Flow of a Nanofluid Past a Stretching Sheet. *J. Sci. Res.* **2014**, *6*, 257–272. [CrossRef]

32.　Poornima, T.; Reddy, N.B. Radiation effects on MHD free convective boundary layer flow of nanofluids over a nonlinear stretching sheet. *Adv. Appl. Sci. Res.* **2013**, *4*, 190–202.

33.　Noor, N.F.M.; Abbasbandy, S.; Hashim, I. Heat and mass transfer of thermophoretic MHD flow over an inclined radiate isothermal permeable surface in the presence of heat source/sink. *Int. J. Heat Mass Transf.* **2012**, *55*, 2122–2128. [CrossRef]

34.　Sheikholeslami, M.; Ganji, D.D.; Javed, M.Y.; Ellahi, R. Effect of thermal radiation on magnetohydrodynamics nanofluid flow and heat transfer by means of two phase model. *J. Magn. Magn. Mater.* **2015**, *374*, 36–43. [CrossRef]

35.　Madhesh, D.; Kalaiselvam, S. Experimental analysis of hybrid nanofluid as a coolant. *Procedia Eng.* **2014**, *97*, 1667–1675. [CrossRef]

36.　Singh, P.; Kumar, M. Mass transfer in MHD flow of alumina water nanofluid over a flat plate under slip conditions. *Alex. Eng. J.* **2015**, *54*, 383–387. [CrossRef]

37.　Rosseland, S. *Astrophysik Und Atom-Theoretische Grundlagen*; Springer: Berlin, Germany, 1931.

38.　Davidson, P.A. *An Introduction to Magnetohydrodynamics*, 1st ed.; Cambridge University Press: New York, NY, USA, 2001.

39.　Abbas, Z.; Naveed, M.; Sajid, M. Heat transfer analysis for stretching flow over a curved surface with magnetic field. *J. Eng. Thermophys.* **2013**, *22*, 337–345. [CrossRef]